University of Bath

Alternative formats

If you require this document in an alternative format, please contact:
openaccess@bath.ac.uk

Page Proof Instructions and Queries

Thank you for choosing to publish with us. This is your final opportunity to ensure your article will be accurate at publication. Please review your proof carefully and respond to the queries using the circled tools in the image below, which are available in Adobe Reader DC* by clicking **Tools** from the top menu, then clicking **Comment**.

Please use *only* the tools circled in the image, as edits via other tools/methods can be lost during file conversion. For comments, questions, or formatting requests, please use ⊺. Please do *not* use comment bubbles/sticky notes ⊙.

*If you do not see these tools, please ensure you have opened this file with **Adobe Reader DC**, available for free at get.adobe.com/reader or by going to Help > Check for Updates within other versions of Reader. For more detailed instructions, please see us.sagepub.com/ReaderXProofs.

Sl. No.	Query
	Please note that we cannot add/amend orcid ids for any article at the proof stage. following orcid's guidelines, the publisher can include only orcid ids that the authors have specifically validated for each manuscript prior to official acceptance for publication.
	Please confirm that all author information, including names, affiliations, sequence, and contact details, is correct.
	Please review the entire document for typographical errors, mathematical errors, and any other necessary corrections; check headings, tables, and figures.
	Please ensure that you have obtained and enclosed all necessary permissions for the reproduction of art works (e.g. illustrations, photographs, charts, maps, other visual material, etc.) not owned by yourself. please refer to your publishing agreement for further information.
	Please note that this proof represents your final opportunity to review your article prior to publication, so please do send all of your changes now.
	Please confirm that the funding and conflict of interest statements are accurate.
1	Please confirm 6th author affiliation
2	Please provide volume for Reference '8'.
3	Please provide page range for Reference '10'.

Analysis of longitudinal-vertical coupling vibration of four hub motors driven electric vehicle under unsteady condition

Qiongyao Li[1], Conggan Ma[1,2], Nic Zhang[3], Yue Guo[4], Michele Degano[5], Chris Gerada[4], Shengsen Zhou[1] and Yuansheng An[1] [AQ: 1]

Abstract

The influence of hub motor unbalanced magnetic force (UMF) on the vibration of electric vehicle under steady state conditions has been known, but under unsteady conditions, the hub motor UMF will change with the vehicle operation condition, and there would exist complex coupling vibration for the hub motors driven electric vehicle. Here, the longitudinal-vertical coupling dynamics of the four hub motors driven electric vehicle under unsteady condition is studied. Integrating the motor electromagnetic excitation and electric vehicle dynamics, a longitudinal-vertical coupling dynamics model of the four hub motors driven electric vehicle is established. Based on the variable switching frequency field-oriented control model, analytical model of the UMFs acting on the motor stator and rotor parts under unsteady condition are developed. For model validation, a four hub motors driven electric vehicle has been tested, the accuracy of the longitudinal-vertical coupling dynamics model established in this paper was verified. Then, longitudinal-vertical coupling vibration characteristics of the four hub motors driven electric vehicle under road excitation and coupling excitation are analyzed. The results show that the longitudinal and vertical movement of the four hub motors driven electric vehicle is coupled by hub motor. In addition, under unsteady condition, the motor UMFs will cause vertical vibration of the electric vehicle body and hub motor stator, the vibration shows order characteristics including low order harmonic hf_c and inverter switching frequency sideband harmonic $k_1 f_s \pm k_2 f_c$ ($f_c = pn/60$, f_s is inverter switching frequency, k_1 and k_2 are positive integers, p is the number of pole pairs and n is motor speed.). The motor electromagnetic torque will cause longitudinal vibration of the electric vehicle body, the vibration shows order characteristics including harmonics $f_s \pm 3f_c$ and $2f_s$. The main harmonic of vehicle body pitch angle acceleration is $2f_s$.

Introduction

In recent years, energy shortage, climate warming, and environmental pollution have become increasingly prominent problems. Energy-saving and environmentally friendly electric vehicles become an important development direction of the automobile industry.[1] For hub motors driven electric vehicle, the motors installed in the wheel hub are used as the prime mover of the electric vehicle. Such electric vehicles have the advantages of short drive chain, efficient transmission, compact structure, high utilization of space inside the vehicle,

[1]School of Automotive Engineering, Harbin Institute of Technology at Weihai, Weihai, Shandong, China
[2]Yangtze River Delta HIT Robot Technology Research Institute, Wuhu, China
[3]Department of Mechanical Engineering, University of Bath, Bath, UK
[4]Coventry University, Coventry, UK
[5]Power Electronics, Machines and Control research group, University of Nottingham, Nottingham, UK

Corresponding author:
Conggan Ma, School of Automotive Engineering, Harbin Institute of Technology at Weihai, 2 West Wenhua Road, Huancui District, Weihai, Shandong 264209, China.
Email: mcg@hit.edu.cn

and independent control of hub motor speed and torque.[2,3] As a result, it has received widespread attention.

One of the topical issues is road and motor induced vehicle vibration. Under road surface excitation or unbalanced load condition, the hub motor may generate eccentricity and further generate unbalanced magnetic force (UMF). The UMF and road excitation will cause vibration of the hub motor stator and rotor parts, and the vibration energy will be transmitted to the wheel and vehicle body, which will affect the handling stability and ride comfort of the electric vehicle. To suppress the vibration of hub motor and electric vehicle, many studies have been conducted. Some novel structures that convert the mass of the hub motor into a mass parallel to the sprung mass or suspended on the vehicle body,[4–6] or two-stage suspension structure[7,8] are proposed to absorb the vibration. Another approach to mitigate the vibration of wheel system and electric vehicle is to optimize the parameters of the motor[9] and the structural parameters of the suspension system.[8,10,11] Different control methods can also be used to reduce the electromagnetic force and improve the ride comfort of electric vehicle.[12–16] With respect to the vibration mechanism of the hub motor driven electric vehicle. Luo and Tan[4] investigated the influence of in-wheel motor UMF on the vehicle vertical dynamics, it found that the UMF will evidently increase the eccentricity and dynamic load, and the novel IWM topology with rubber bushing proposed in this paper can observably improve the vehicle dynamics. Literature[17,18] studied the influence of hub motor UMF on the vehicle vertical and lateral dynamics, and the vehicle dynamics under different constant vehicle speeds,[17] it shows that the UMF has negative impact on the vertical and lateral dynamics of the vehicle, and the dynamic performance of electric vehicle deteriorates with the increase of vehicle speed. Yu et al.[19] explored the effects of motor UMF and bearing nonlinear force on the vibration characteristics of hub motors driven electric vehicle. It found that the rotor-bearing coupling vibration mainly affects the tire vibration acceleration and tire dynamic load. The forces of the motor in x and z directions are obtained in stator coordinate system. Literature[20,21] investigated the influence of road surface and UMF on the vehicle dynamics, it found that the motor eccentricity, UMF and road roughness are highly coupled.[20,21] Considering the dynamic coupling between the hub motor electromagnetic excitation and transient dynamics of electric vehicle, Li et al.[22] established an electromechanical coupling model of hub motor driven electric vehicle, and analyzed the vibration transfer characteristics of electric vehicle to the UMF. The UMFs acts on the stator and rotor are considered to be equal in magnitude and opposite in direction, and it found that the UMF causes the second-order resonates, especially for the unsprung mass. Wu et al.[10] established a mechanical-electrical-magnetic coupling model for a hub motor driven electric vehicle considering the strong coupling effect between motor eccentricity and

UMF, and analyzed its influence on the vehicle performance. The UMFs acting on the stator and rotor are considered as a pair of internal force. In fact, the UMFs acting on the hub motor stator and rotor parts are not a pair of internal force, the frequency characteristics of the UMFs are different. The frequency characteristics of UMF acting on the stator is related to the number of pole pairs and motor speed. Calculating the UMF acting on the rotor usually assumes that the rotor does not move and the stator rotates in the opposite direction, so the frequency characteristics of UMF acting on the rotor is related to the number of stator slots and motor speed. Literature[23,24] prove that the UMFs acting on the motor stator and rotor are not a pair of internal forces, so it is necessary to calculate the UMFs acting on the hub motor stator and rotor parts respectively.

The above mentioned studies mainly focused on the steady state conditions at constant vehicle speeds. Meanwhile, electric vehicle in reality would work mostly under unsteady conditions, such as launching, acceleration and deceleration, etc. The characteristics of hub motor UMFs will change with the vehicle operation condition, resulting in the change of hub motor excitation to the wheel and vehicle body. Therefore, it is necessary to study the coupling vibration characteristics of four hub motors driven electric vehicle under unsteady condition. Sun et al.[25] built a quarter vehicle dynamic model and found that the hub motor UMF will have a negative effect on the electric vehicle dynamics under starting condition. Mao et al. investigated the longitudinal vibration of electric wheel system under the starting condition of vehicle speed from 0 to 6 m/s,[26] acceleration condition of motor speed from 0 to 200 r/min[27] and motor speed from 0 to 300 r/min,[28,29] and a method based on BP neural network is proposed to suppress the longitudinal vibration of the electric wheel system.[9] Hu et al.[12] established the electromechanical coupling model for the electric vehicle with the switched reluctance motor as the hub motor, and developed a controller to improve the dynamic performance of the electric vehicle. However, the difference in frequency characteristics of UMFs acting on stator and rotor are not considered.

Given the above, the existing literature indicate the following problems to be further improved:

(1) Most of the existing literature regard the hub motor UMFs as an internal force, which act on the stator and rotor parts with the same amplitude and in opposite directions. However, the frequency characteristics of UMFs acting on the motor stator and rotor parts are different due to the different frequency characteristics of permanent magnet field and armature reaction magnetic field on the stator and rotor,[23,24] so it is necessary to calculate the UMFs acting on the hub motor stator and rotor parts respectively.
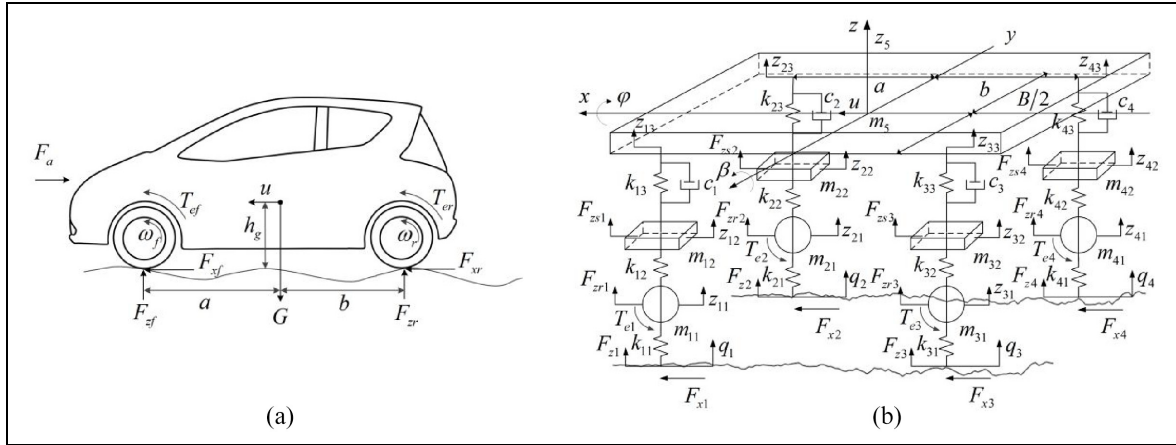
Figure 1. Force diagram and dynamics model of four hub motors driven electric vehicle: (a) force diagram and (b) longitudinal-vertical coupling dynamics model.

(2) Under unsteady condition and road surface random excitation, the speed, driving torque demands and eccentricity of the hub motors are different, which leads to different electromagnetic excitations to the wheels and vehicle body. Different from the electric wheel system, the left and right sides, front and rear axles of the electric vehicle are closely coupled in operation. Therefore, it is necessary to consider the transient electromechanical coupling of the electromagnetic force, and study the longitudinal-vertical coupling vibration characteristics of the four hub motors driven electric vehicle under unsteady condition.

In this paper, four hub motors driven electric vehicle is taken as the research subject, the contribution of this article is to establish the dynamics model for the longitudinal and vertical coupling of four hub motors driven electric vehicle under unsteady condition, considering the transient electromechanical coupling of the electromagnetic force. The effect of the hub motor UMFs on the vibration of the four hub motors driven electric vehicle under unsteady condition can be analyzed by using the proposed model, considering the difference of the UMFs acting on the hub motor stator and rotor parts. The accuracy of the longitudinal-vertical coupling dynamics model established in this paper is verified by the electric vehicle acceleration test.

Dynamics model of four hub motors driven electric vehicle

Longitudinal-vertical coupling dynamics model

In order to investigate the longitudinal-vertical coupling vibration characteristics of four hub motors driven electric vehicle, a longitudinal-vertical coupling dynamics model of electric vehicle under coupling excitation of road roughness and UMFs is established, as shown in Figure 1.

The major assumptions of this model are as follows:

(1) Roll angle and pitch angle of the vehicle body are small.
(2) Bearing stiffness, suspension stiffness and damping are all linear.
(3) The tires are always in contact with the road surface.
(4) The stiffness and damping of the tire are ignored.

In Figure 1(b), φ and β are the roll angle and pitch angle of vehicle body respectively, q_i ($i = 1,2,3,4$ represents left front, right front, left rear and right rear respectively) is the displacement of road roughness, z_5, z_{i1}, z_{i2}, z_{i3} are the vertical displacements of vehicle body, motor rotor part, motor stator part and joint of suspension respectively, T_{ei} is the electromagnetic torque of hub motor, ω_i is the mechanical speed of wheel, F_{xi} and F_{zi} are the longitudinal force and vertical force of the wheel respectively, F_{xi} can be obtained by using equation (9). F_{zsi} and F_{zri} are the vertical UMFs acting on hub motor stator and rotor parts respectively, when $F_{zsi} = F_{zri} = 0$, the dynamic model is longitudinal-vertical coupling dynamics model under only road excitation. m_5, m_{i1}, m_{i2}, c_i, k_{i1}, k_{i2}, k_{i3} and B are shown in Table 1.

Vibration equations

According to Newton's second law, the dynamics equations of the longitudinal-vertical coupling dynamics model shown in Figure 1(b) can be obtained.

Longitudinal movement equation of the four hub motors driven electric vehicle is

$$m(\ddot{x} + \dot{z}_5\dot{\beta}) = m_5 h_s \ddot{\beta} + F_{x1} + F_{x2} + F_{x3} + F_{x4} - F_a \tag{1}$$

where F_a is the air resistance, $F_a = C_D A u^2/21.15$, u is the vehicle driving speed, C_D is air resistance coefficient, A is the frontal area.

Roll movement equation of the vehicle body is

Table 1. Main parameters of four hub motors driven electric vehicle.

Symbol	Parameter	Value	Unit
m	Vehicle mass	1343	kg
m_5	Sprung mass	1103	kg
m_{i1}	Mass of hub motor rotor and tire	40	kg
m_{i2}	Mass of hub motor stator and shaft	20	kg
I_{xx}	Roll moment of inertia of the vehicle body about x-axis	620	kg·m^2
I_{yy}	Pitch moment of inertia of the vehicle body about y-axis	1480	kg·m^2
k_{i1}	Tire stiffness	210	kN/m
k_{i2}	Hub motor bearing stiffness	4000	kN/m
k_{13}, k_{23}	Front suspension stiffness	20	kN/m
k_{33}, k_{43}	Rear suspension stiffness	24	kN/m
c_1, c_2	Front suspension damping	4000	N·s/m
c_3, c_4	Rear suspension damping	4200	N·s/m
a	Distance between vehicle mass center and front axle	1.158	m
b	Distance between vehicle mass center and rear axle	1.147	m
l	Wheel base	2.305	m
B	Wheel track	1.398	m
h_s	Distance between the body mass center and pitch axis	0.488	m
h_g	Height of body mass center	0.52	m
r_w	Wheel rolling radius	0.29	m

$$I_{xx}\ddot{\varphi} - m_5 g h_s \varphi + \begin{bmatrix} c_1(\dot{z}_{13} - \dot{z}_{12}) + k_{13}(z_{13} - z_{12}) + \\ c_3(\dot{z}_{33} - \dot{z}_{32}) + k_{33}(z_{33} - z_{32}) \end{bmatrix} B/2 - \begin{bmatrix} c_2(\dot{z}_{23} - \dot{z}_{22}) + k_{23}(z_{23} - z_{22}) + \\ c_4(\dot{z}_{43} - \dot{z}_{42}) + k_{43}(z_{43} - z_{42}) \end{bmatrix} B/2 = 0 \tag{2}$$

Pitch movement equation of the vehicle body is

$$I_{yy}\ddot{\beta} + m_5 \ddot{x} h_s - \begin{bmatrix} c_1(\dot{z}_{13} - \dot{z}_{12}) + k_{13}(z_{13} - z_{12}) + \\ c_2(\dot{z}_{23} - \dot{z}_{22}) + k_{23}(z_{23} - z_{22}) \end{bmatrix} a + \begin{bmatrix} c_3(\dot{z}_{33} - \dot{z}_{32}) + k_{33}(z_{33} - z_{32}) + \\ c_4(\dot{z}_{43} - \dot{z}_{42}) + k_{43}(z_{43} - z_{42}) \end{bmatrix} b = 0 \tag{3}$$

where,

$$z_{13} = z_5 + B\varphi/2 - a\beta$$

$$z_{23} = z_5 - B\varphi/2 - a\beta$$

$$z_{33} = z_5 + B\varphi/2 + b\beta$$

$$z_{43} = z_5 - B\varphi/2 + b\beta \tag{4}$$

Vertical movement equation of the sprung mass is

$$m_5(\ddot{z}_5 - \dot{x}\dot{\beta}) + c_1(\dot{z}_{13} - \dot{z}_{12}) + c_2(\dot{z}_{23} - \dot{z}_{22}) + c_3(\dot{z}_{33} - \dot{z}_{32}) + c_4(\dot{z}_{43} - \dot{z}_{42}) + k_{13}(z_{13} - z_{12}) + k_{23}(z_{23} - z_{22}) + k_{33}(z_{33} - z_{32}) + k_{43}(z_{43} - z_{42}) = 0 \tag{5}$$

Vertical movement equation of the unsprung mass is

$$m_{i1}\ddot{z}_{i1} + k_{i1}(z_{i1} - q_i) - k_{i2}(z_{i2} - z_{i1}) = F_{zri} \tag{6}$$

$$m_{i2}\ddot{z}_{i2} + k_{i2}(z_{i2} - z_{i1}) - c_i(\dot{z}_{i3} - \dot{z}_{i2}) - k_{i3}(z_{i3} - z_{i2}) = F_{zsi} \tag{7}$$

Driving equation

The movement equation of the electric vehicle wheel can be expressed as

$$T_{ei} - F_{xi}r_w = I_i\dot{\omega}_i \tag{8}$$

where T_{ei} is the electromagnetic torque of hub motor, F_{xi} is the tire longitudinal force, I_i is the rotational inertia of the wheel, ω_i is the mechanical speed of wheel.

Tire model

The Magic Formula model[30] is used to obtain the tire longitudinal forces F_{xi} in the equation (1). Under pure longitudinal slip condition, the tire longitudinal force is

$$F_x = D_x \sin(C_x \arctan(B_x s_x - E_x(B_x s_x - \arctan(B_x s_x)))) + S_{Vx} \tag{9}$$

where $s_x = s + S_{Hx}$, $s = -v_{sx}/|u|$ is longitudinal slip ratio, $v_{sx} = u - r_w\omega$ is slip velocity, $D_x = \mu_x F_z$ is longitudinal force peak value, $C_x = P_{Cx1}$ is the shape factor, $B_x = K_{xk}/(C_x D_x + \varepsilon_x)$ is the stiffness factor, $E_x = (P_{Ex1} + P_{Ex2}df_z + P_{Ex3}df_z^2)[1 - P_{Ex4}\,\mathrm{sgn}(s_x)]$ is the curvature factor, $S_{Hx} = P_{Hx1} + P_{Hx2}df_z$ and $S_{Vx} = P_{Vx1} + P_{Vx2}df_z$ are the horizontal and vertical shift respectively, $\mu_x = P_{Dx1} + P_{Dx2}df_z$ is the friction coefficient, $K_{xk} = F_z(P_{Kx1} + P_{Kx2}df_z)e^{P_{Kx3}df_z}$, $df_z = (F_z - F_{z0})/F_{z0}$ is wheel vertical load change, F_z and F_{z0} are wheel vertical load under operation and stationary condition.

Wheel vertical load model

The wheel vertical load under operation condition is included in the tire model, and it can be expressed as

$$F_{z1} = m_5 g b/2l + (m_{11} + m_{12})g - k_{11}(z_{11} - q_1) \quad (10)$$

$$F_{z2} = m_5 g b/2l + (m_{21} + m_{22})g - k_{21}(z_{21} - q_2) \quad (11)$$

$$F_{z3} = m_5 g a/2l + (m_{31} + m_{32})g - k_{31}(z_{31} - q_3) \quad (12)$$

$$F_{z4} = m_5 g a/2l + (m_{41} + m_{42})g - k_{41}(z_{41} - q_4) \quad (13)$$

Road excitation and UMFs excitation model

Road excitation model

The road excitation model of the left front wheel can be expressed as[17]

$$\dot{q}_1(t) = -2\pi n_c u q_1(t) + 2\pi n_0 \sqrt{G_0(n_0)u}w(t) \quad (14)$$

where $q(t)$ is road roughness displacement, n_c is a low cutoff space frequency, n_0 is reference space frequency, $G_0(n_0)$ is road roughness coefficient, $w(t)$ is white noise, u is vehicle speed.

Considering the correlation of four wheels road excitations, the road roughness inputs of four wheels can be expressed as[17]

$$\dot{Q}(t) = AQ(t) + B_0 w(t) \quad (15)$$

where,

$$Q(t) = \begin{bmatrix} q_1(t) & q_2(t) & q_3(t) & q_4(t) & x_1(t) & x_2(t) \end{bmatrix}^{\mathrm{T}}$$

$$A = \begin{bmatrix} -2\pi n_c u & 0 & 0 & 0 & 0 & 0 \\ -2\pi n_c u - 12u/B & 0 & 0 & 0 & 0 & 1 \\ 2\pi n_c u + 2u/l & 0 & -2u/l & 0 & 0 & 0 \\ 2\pi n_c u + 12u/B & 2u/l & 0 & -2u/l & 0 & -1 \\ -12u/B & 0 & 0 & 0 & 0 & 1 \\ 72u^2/B^2 & 0 & 0 & 0 & -12u^2/B^2 & -6u/B \end{bmatrix}$$

$$B_0 = \begin{bmatrix} C & C & -C & -C & 0 & 0 \end{bmatrix} C = 2\pi n_0 \sqrt{G_0(n_0)u}$$

$$\begin{bmatrix} \dot{x}_1 \\ \dot{x}_2 \end{bmatrix} = \begin{bmatrix} 0 & 1 \\ -\frac{12u^2}{B^2} & -\frac{6u}{B} \end{bmatrix} \begin{bmatrix} x_1 \\ x_2 \end{bmatrix} + \begin{bmatrix} -\frac{12u}{B} \\ \frac{72u^2}{B^2} \end{bmatrix} q_1(t) \quad (16)$$

UMFs model of the hub motor

Control model of external rotor PMSM. In order to obtain the UMFs of the hub motor under unsteady condition, the three phase currents need to be obtained first, so the field-oriented control (FOC) model of the external rotor PMSM is established. The dead time is considered in the FOC model. In addition, the variable switching frequency technology is adopted, as shown in
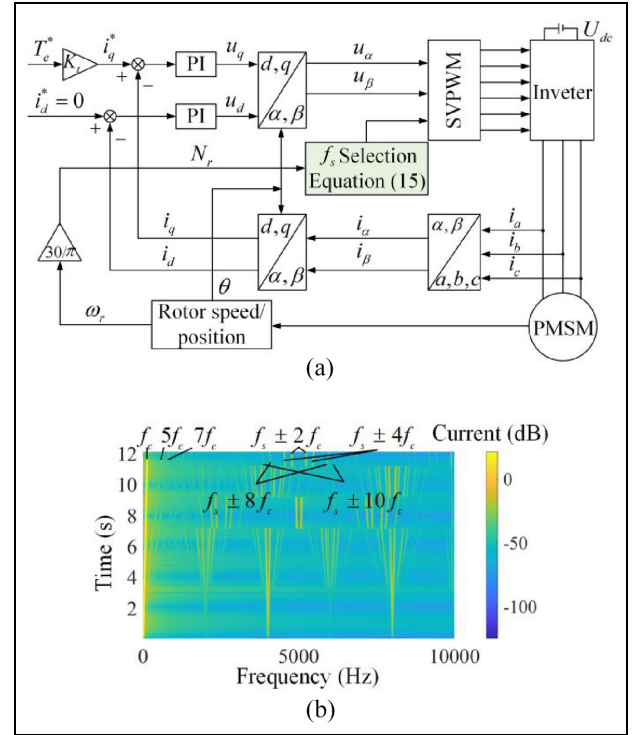

Figure 2. (a) Variable switching frequency FOC diagram and (b) time-frequency map of phase current simulation result.

Figure 2(a). The switching frequency corresponding to the real-time motor speed n is shown as

$$f_s = \begin{cases} 2000\mathrm{Hz} & n < 350\mathrm{rpm} \\ 2500\mathrm{Hz} & 350\mathrm{rpm} \leqslant n < 450\mathrm{rpm} \\ 4000\mathrm{Hz} & 450\mathrm{rpm} \leqslant n < 550\mathrm{rpm} \\ 5000\mathrm{Hz} & 550\mathrm{rpm} \leqslant n < 664\mathrm{rpm} \\ 6250\mathrm{Hz} & 664\mathrm{rpm} \leqslant n \end{cases} \quad (17)$$

Due to the dead time effect and pulse width modulation, harmonic currents will be introduced to the three phase currents.[24,26] The harmonic currents are mainly composed of low order harmonics $(6k \pm 1)f_c$ and inverter switching frequency sideband harmonic $k_1 f_s \pm k_2 f_c$, where $f_c = pn/60$, $k = 1, 2, 3, \ldots$.

Based on the FOC model of external rotor PMSM, the time-frequency map of phase current under acceleration condition can be obtained, as shown in Figure 2(b). It can be seen that the phase current show order features, the main harmonics are f_c, $5f_c$, $7f_c$, $f_s \pm 2f_c$, $f_s \pm 4f_c$, $f_s \pm 8f_c$ and $f_s \pm 10f_c$. The frequency of phase current harmonics related to switching frequency varies with motor speed, and they are discontinuous.

UMFs model. Figure 3 depicts the motor eccentricity in stator and rotor coordinate system. It is assumed that the eccentricity direction is in the vertical direction, e is motor eccentricity, which can be obtained by the dynamics model of electric vehicle, o_r and o_r' are geometric center of rotor in stator and rotor coordinate
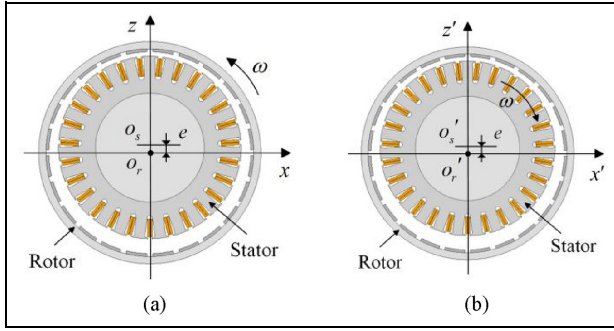
Figure 3. Eccentricity in two coordinate systems: (a) stator coordinate system and (b) rotor coordinate system.

system respectively, o_s and o_s' are the geometric center of stator in two coordinate system respectively.

The eccentricity of the external rotor PMSM is

$$e_i(t) = z_{i2} - z_{i1} \tag{18}$$

According to Figure 3, the air gap of the external rotor PMSM with eccentricity in stator and rotor coordinate system are

$$\delta_s(\alpha) = \delta - e\cos(\alpha - \pi/2) \tag{19}$$

$$\delta_r(\theta, \alpha) = \delta - e\cos(\theta + \alpha - \pi/2) \tag{20}$$

where $\delta = \delta_0 + h_m/\mu_r$ is the effective air gap length, δ_0 is airgap length, h_m is the thickness of permanent magnet, μ_r is the relative permeability, α is the circumferential angle of the motor, θ is the integral of motor speed.

The air gap permeance of the external rotor PMSM with eccentricity in stator coordinate system is

$$\lambda_s(\alpha) = \frac{\mu_0}{\delta_s(\alpha)} = \frac{\mu_0}{\delta}\frac{1}{1 - \varepsilon\cos(\alpha - \pi/2)} = \lambda\varepsilon_s(\alpha) \tag{21}$$

where ε_s is magnetic permeance correction coefficient of eccentricity, $\varepsilon = e/\delta$ is effective eccentricity ratio, λ is magnetic permeance without eccentricity.

Considering only the first two orders, the Fourier series of ε_s in stator coordinate system is

$$\varepsilon_s(\alpha) = \frac{1}{\sqrt{1 - \varepsilon^2}} + \frac{2}{\sqrt{1 - \varepsilon^2}}\frac{1 - \sqrt{1 - \varepsilon^2}}{\varepsilon}\cos(\alpha - \pi/2) \tag{22}$$

In the same way, the magnetic permeance correction coefficient of eccentricity in rotor coordinate system is

$$\varepsilon_r(\theta, \alpha) =$$
$$\frac{1}{\sqrt{1 - \varepsilon^2}} + \frac{2}{\sqrt{1 - \varepsilon^2}}\frac{1 - \sqrt{1 - \varepsilon^2}}{\varepsilon}\cos(\theta + \alpha - \pi/2) \tag{23}$$

where ε_r is magnetic permeance correction coefficient of eccentricity in rotor coordinate system, r represents the rotor coordinate system.

The magnetic force density of external rotor PMSM with eccentricity in stator and rotor coordinate system can be obtained by Maxwell tensor method.

$$p_{ers}(r, \theta, \alpha) = \frac{1}{2\mu_0}\left[B_{rs}^2(r, \theta, \alpha) - B_{ts}^2(r, \theta, \alpha)\right]\varepsilon_s^2(\alpha) \tag{24}$$

$$p_{ets}(r, \theta, \alpha) = \frac{1}{\mu_0}B_{rs}(r, \theta, \alpha)B_{ts}(r, \theta, \alpha)\varepsilon_s^2(\alpha) \tag{25}$$

$$p_{err}(r, \theta, \alpha) = \frac{1}{2\mu_0}\left[B_{rr}^2(r, \theta, \alpha) - B_{tr}^2(r, \theta, \alpha)\right]\varepsilon_r^2(\theta, \alpha) \tag{26}$$

$$p_{etr}(r, \theta, \alpha) = \frac{1}{\mu_0}B_{rr}(r, \theta, \alpha)B_{tr}(r, \theta, \alpha)\varepsilon_r^2(\theta, \alpha) \tag{27}$$

where B_{rs} and B_{ts} are radial and tangential air gap magnetic fields in the stator coordinate system, B_{rr} and B_{tr} are radial and tangential air gap magnetic fields in the rotor coordinate system. The air gap magnetic fields can be obtained by permanent magnetic field and armature reaction magnetic field.[23]

The vertical UMF acting on the motor stator part can be obtained by

$$F_{zs}(r, \theta) = lr\int_0^{2\pi}\left(\begin{array}{c}p_{ers}(r, \theta, \alpha)\sin\alpha + \\ p_{ets}(r, \theta, \alpha)\cos\alpha\end{array}\right)d\alpha \tag{28}$$

To obtain the UMF acting on the motor rotor part in the vertical direction of vehicle coordinate system, the angle θ should be considered in the integration.

$$F_{zr}(r, \theta) = lr\int_0^{2\pi}\left(\begin{array}{c}p_{err}(r, \theta, \alpha)\sin(\theta + \alpha) + \\ p_{etr}(r, \theta, \alpha)\cos(\theta + \alpha)\end{array}\right)d\alpha \tag{29}$$

Analysis of the hub motor UMFs. Ignoring the force direction, UMFs acting on the motor stator and rotor parts under acceleration condition are shown in Figure 4. It can be seen that the UMFs acting on the motor stator and rotor parts increase with the increase of motor speed, they have almost the same varying trend (Figure 4(a)), but the frequency characteristics are different (Figure 4(b) and (c)). The main harmonics of the stator part are $2f_c$, $4f_c$, $6f_c$, $8f_c$, $10f_c$, $12f_c$, $f_s \pm f_c$, $f_s \pm 3f_c$ and $f_s \pm 9f_c$, the main harmonics of motor rotor part are $Q_s f_r$ (Q_s is the number of stator slot), $2Q_s f_r$, $3Q_s f_r$, $f_s \pm 9f_r$, $f_s \pm 3f_c$, and $f_s \pm 9f_c$. UMFs acting on the motor stator and rotor parts both contain harmonics of $f_s \pm 3f_c$ and $f_s \pm 9f_c$, it is because that these harmonics
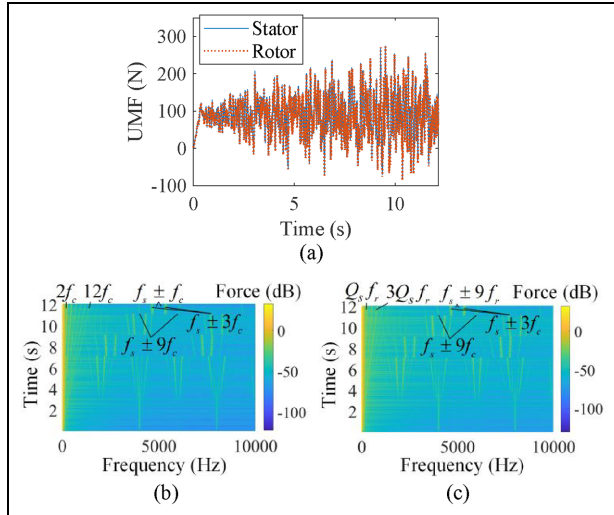
Figure 4. UMFs act on the hub motor stator and rotor parts: (a) time domain, (b) time-frequency map of UMF act on the motor stator, and (c) time-frequency map of UMF act on the motor rotor.
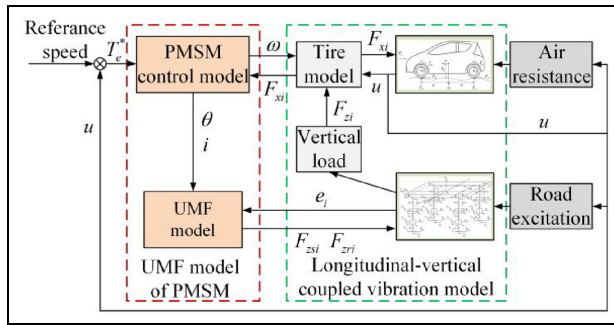

Figure 5. Logic diagram of longitudinal-vertical coupling dynamics model under coupling excitation.

corresponding to the UMFs generated by 0-order electromagnetic force.[24]

Longitudinal-vertical coupling dynamics analysis of four hub motors driven electric vehicle under acceleration condition

According to the longitudinal-vertical coupling dynamics equations of the four hub motors driven electric vehicle, the longitudinal-vertical coupling simulation model under road excitation and coupling excitation of road roughness and UMFs can be established, using Matlab/Simulink. The strong coupling effect between the motor eccentricity and UMFs is considered. Logic diagram of longitudinal-vertical coupling model of the four hub motors driven electric vehicle under coupling excitation is shown in Figure 5.

The expected electromagnetic torque of the hub motor can be obtained based on the actual and expected speed of the electric vehicle. The mechanical speed of the hub motor can be obtained by the PMSM
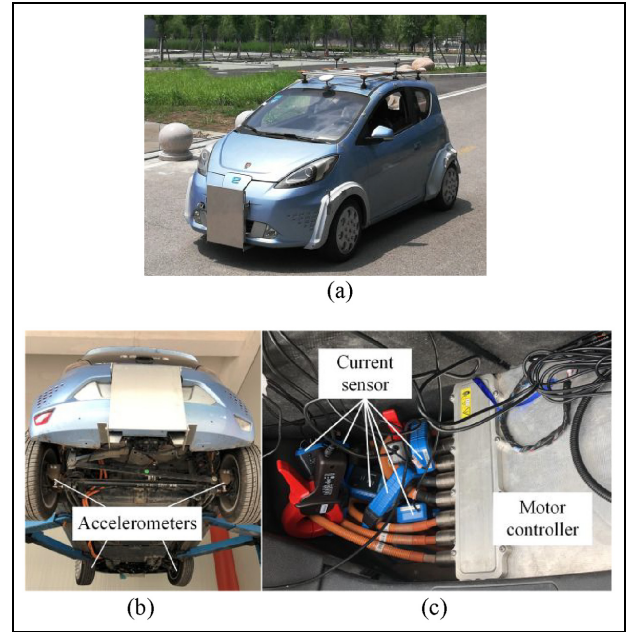

Figure 6. Tested electric vehicle and sensors arrangement: (a) four hub motors driven electric vehicle, (b) accelerometers arrangement, and (c) current sensors arrangement.

control model, based on the expected electromagnetic torque and the actual load torque. The slip rate of the tire can be obtained based on the mechanical speed of the hub motor and the speed of the four hub motors driven electric vehicle. Taking into account the changes in the vertical load of the wheels, the tire longitudinal forces can be calculated based on the tire model. The longitudinal forces will drive the four hub motors driven electric vehicle to achieve acceleration, uniform speed, deceleration and other operating conditions.

The input of the UMF model is the real-time three-phase currents and rotor angle of the hub motor, as well as the real-time eccentricities between the stator and rotor of the four hub motors obtained from the vibration model. The transient UMFs acting on the motor stator and rotor are calculated respectively, using the analytical model of the UMF of the external rotor PMSM. The influence of UMF on the vibration characteristics of the four hub motors driven electric vehicle under unsteady condition can be analyzed, using the longitudinal-vertical coupling simulation platform of the four hub motors driven electric vehicle.

Verification of the dynamics model

To verify the established longitudinal-vertical coupling dynamics model, a real vehicle dynamic test was carried out on a four hub motors driven electric vehicle. Figure 6 shows the tested electric vehicle and the arrangement of the sensors. Accelerometers were arranged on the wheel stator parts and the vehicle body, the type of the accelerometer is INV9824, and the available frequency is 1–15 k. The six current
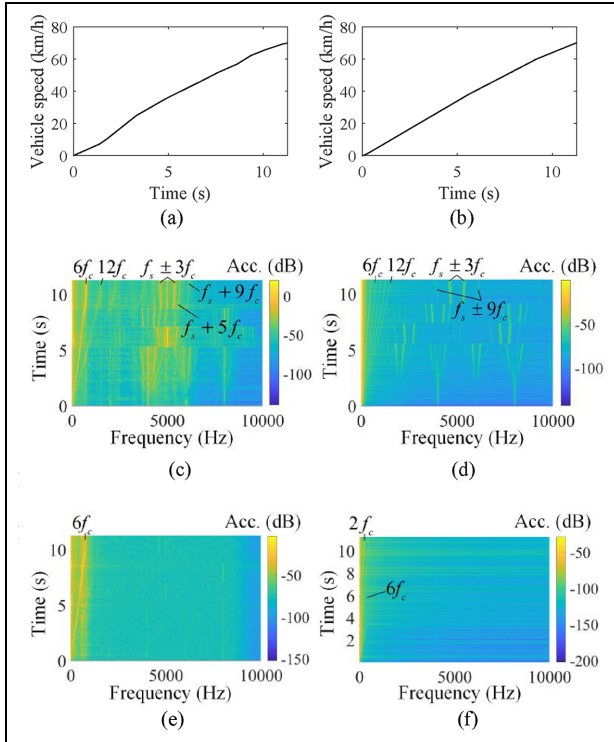
Figure 7. Vehicle speed, vertical vibration acceleration of wheel stator part and vehicle body: (a) tested vehicle speed, (b) simulated vehicle speed, (c) experimental result of wheel stator part, (d) simulated result of wheel stator part, (e) experimental result of vehicle body, and (f) simulated result of vehicle body.

Figure 8. The experimental and simulated current time-frequency maps: (a) experimental current and (b) simulated current.

Table 2. Frequency of the UMFs induced by the fundamental permanent magnet field and current harmonics around the first carrier frequency.

Current harmonics	Frequency of 0-order UMF	Frequency of N_t-order UMF
$f_s + 2f_c$	$f_s + 3f_c$	$f_s + f_c$
$f_s - 2f_c$	$f_s - 3f_c$	$f_s - f_c$
$f_s + 4f_c$	$f_s + 3f_c$	$f_s + 5f_c$
$f_s - 4f_c$	$f_s - 3f_c$	$f_s - 5f_c$
$f_s + 8f_c$	$f_s + 9f_c$	$f_s + 7f_c$
$f_s - 8f_c$	$f_s - 9f_c$	$f_s - 7f_c$
$f_s + 10f_c$	$f_s + 9f_c$	$f_s + 11f_c$
$f_s - 10f_c$	$f_s - 9f_c$	$f_s - 11f_c$

sensors were arranged through the three phase wires of the left rear and right rear hub motors, the type of the current sensor is CC650. Data acquisition was used to collect the experimental data, and the type is DH5902.

During the test, the electric vehicle accelerates from 0 to 70 km/h. Figure 7(a) and (b) shows the experimental and simulated vehicle speeds. The vertical vibration acceleration experimental result and simulated result of the wheel stator part are shown in Figure 7(c) and (d). There are obvious order features in the time-frequency maps, the main harmonics of experimental result are $6f_c$, $12f_c$, f_s, $f_s \pm 3f_c$, $f_s + 5f_c$, and $f_s + 9f_c$, and the main harmonics of simulated result are $2f_c$, $4f_c$, $6f_c$, $8f_c$, $10f_c$, $12f_c$, $f_s \pm 3f_c$, and $f_s \pm 9f_c$. The vertical vibration acceleration experimental result and simulated result of the vehicle body are shown in Figure 7(e) and (f). The main harmonics of experimental result is $6f_c$, and the main harmonics of simulated result are $2f_c$, $4f_c$, and $6f_c$. The main harmonics of the simulated result are basically consistent with the experimental result, the accuracy of the longitudinal-vertical coupling model established in this paper can be verified.

The harmonics in the time-frequency maps of the vertical vibration acceleration of wheel stator part and vehicle body are mainly caused by the hub motor UMF excitation, which is generated by the interaction of the permanent magnet magnetic field and the armature reaction magnetic field. The armature reaction magnetic field is related to the current. Figure 8 shows the
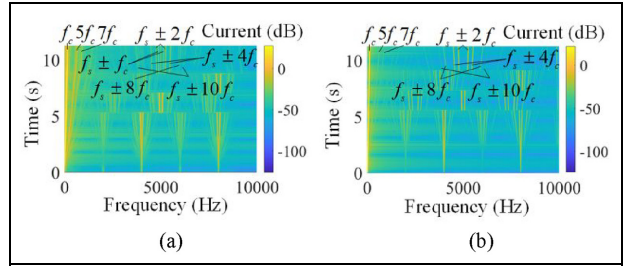
time-frequency maps of experimental current and simulated current. The main harmonics of the experimental current in the low frequency range are mainly f_c, $5f_c$ and $7f_c$, while the main harmonics in the high frequency range are $f_s \pm f_c$, $f_s \pm 2f_c$, $f_s \pm 4f_c$, $f_s \pm 8f_c$, and $f_s \pm 10f_c$. The main harmonics of the simulated current in the low frequency range are mainly f_c, $5f_c$, and $7f_c$, while the main harmonics in the high frequency range are $f_s \pm 2f_c$, $f_s \pm 4f_c$, $f_s \pm 8f_c$, and $f_s \pm 10f_c$. Compared with the simulated current, the experimental current has an additional harmonic of $f_s \pm f_c$.

In the low frequency range, the harmonics of the permanent magnet magnetic field are f_c, $3f_c$, $5f_c$, etc., and the harmonics of the armature reaction magnetic field are f_c, $5f_c$, $7f_c$, etc. According to the Maxwell stress tensor method, the frequency components of the UMF generated by the interaction of the permanent magnet magnetic field and the armature reaction magnetic field are $2f_c$, $4f_c$, $6f_c$, $8f_c$, $10f_c$, $12f_c$, etc., which is consistent with the simulated result. Due to the large amplitude of the experimental current harmonics of $5f_c$ and $7f_c$, the harmonics of $6f_c$ and $12f_c$ in the wheel stator vertical vibration acceleration are obvious, and the harmonic of $6f_c$ in the vehicle vertical vibration acceleration is obvious.

In the high frequency range, the frequency of the current harmonics around the first carrier frequency is theoretically $f_s \pm 2kf_c$. Table 2 shows the frequencies of the 0-order and N_t-order (N_t is the number of unit motor) UMFs generated by the interaction of current
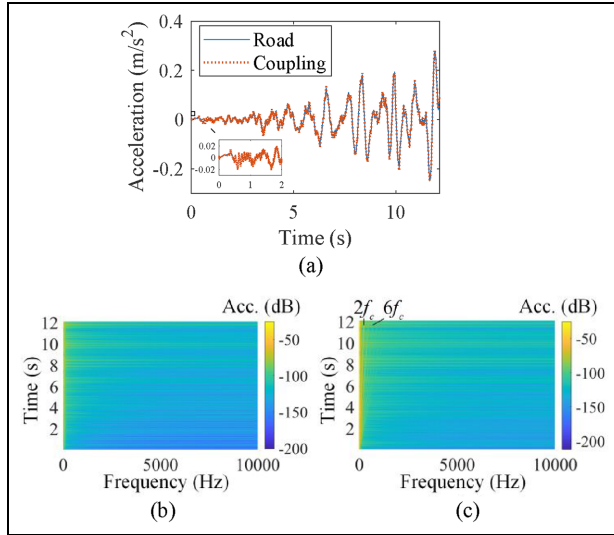
Figure 9. Vehicle body vertical acceleration: (a) time domain, (b) time-frequency map under road excitation, and (c) time-frequency map under coupling excitation.

Figure 10. Suspension deflection: (a) time domain, (b) time-frequency map under road excitation, and (c) time-frequency map under coupling excitation.

harmonics $f_s \pm 2kf_c$ with the fundamental permanent magnet field.

In the simulated vertical vibration acceleration of wheel stator part, the harmonics of $f_s \pm 3f_c$ and $f_s \pm 9f_c$ (0-order) are obvious, while the UMF with the harmonics of $f_s \pm f_c$, $f_s \pm 5f_c$, $f_s \pm 7f_c$ and $f_s \pm 11f_c$ (N_t-order) are relatively not obvious. For the experimental vertical vibration acceleration of wheel stator part, except for $f_s - 9f_c$ (0-order), the harmonics of $f_s \pm 3f_c$ and $f_s + 9f_c$ (0-order) are obvious, it is mainly because the current harmonics of $f_s - 8f_c$ and $f_s - 10f_c$ that generate the UMF harmonics of $f_s - 9f_c$ are not obvious. The UMF with the harmonic of $f_s + 5f_c$ (N_t-order) is also obvious. In addition, there is also a harmonic of f_s (0-order) in the experimental wheel stator part time-frequency map, it is mainly caused by the current experimental harmonics of $f_s \pm f_c$ (additional harmonic compared to simulated current), which also generate UMF of $f_s + 2f_c$ and $f_s - 2f_c$ (N_t-order), but they are not obvious.

Influence of the hub motor UMFs on the vehicle dynamics

In this section, the electric vehicle accelerates from 0 to 65 km/h with uniform acceleration of 1.5 m/s² on B-class road, the vehicle body vertical acceleration, suspension deflection, stator vertical acceleration, motor eccentricity, vehicle body longitudinal acceleration and vehicle body pitch angle acceleration can be obtained by the simulation model. The vehicle body vertical acceleration, suspension deflection, motor stator vertical acceleration, motor rotor vertical acceleration and motor eccentricity under road excitation and coupling excitation are shown in Figures 9 to 13.

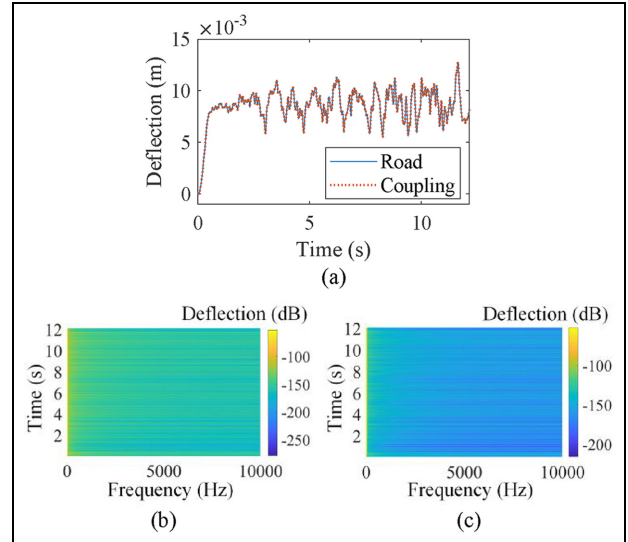From the time domain, the vehicle body vertical acceleration, suspension deflection, stator vertical
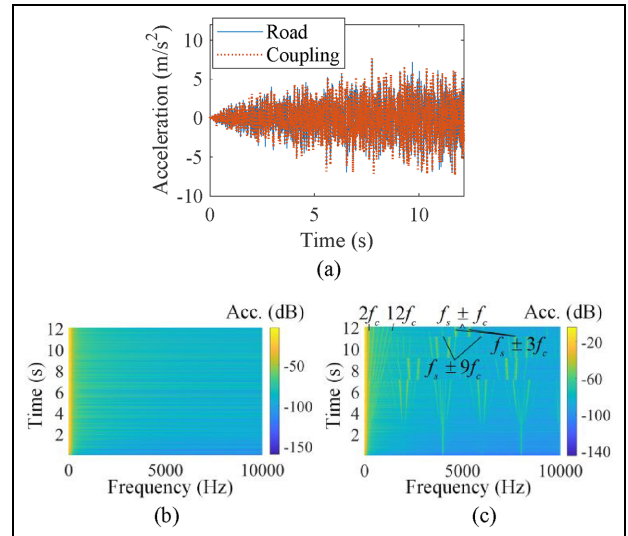

Figure 11. Motor stator vertical acceleration: (a) time domain, (b) time-frequency map under road excitation, and (c) time-frequency map under coupling excitation.

acceleration, rotor vertical acceleration and motor eccentricity fluctuate more strongly with the increase of vehicle speed. The UMFs obviously aggravate the hub motor eccentricity at low speed and have some effect on the stator vertical acceleration and vehicle body vertical acceleration, but have slight effect on the suspension deflection. In time-frequency maps, there is basically no difference in the frequency characteristics of suspension deflection and motor eccentricity under road excitation and coupling excitation. The vehicle body vertical vibration under coupling excitation exhibit order features obviously, and the main harmonics are $2f_c$, $4f_c$, $6f_c$. The stator vertical vibration under coupling excitation mainly occurs at $2f_c$, $4f_c$, $6f_c$, $8f_c$, $10f_c$, $12f_c$, $f_s \pm f_c$,
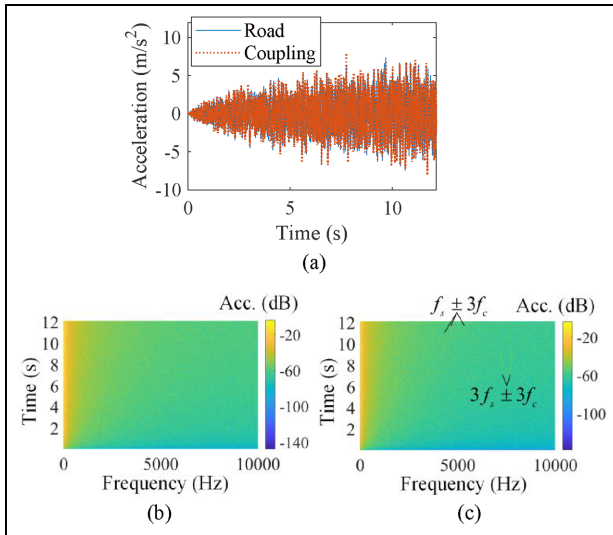
Figure 12. Motor rotor vertical acceleration: (a) time domain, (b) time-frequency map under road excitation, and (c) time-frequency map under coupling excitation.
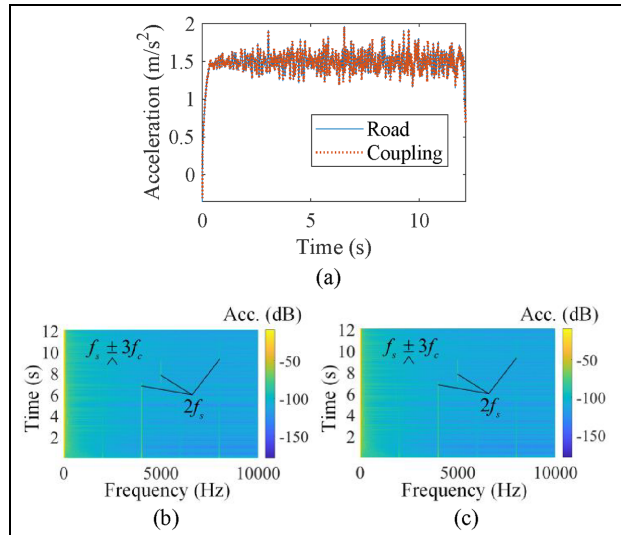

Figure 14. Vehicle body longitudinal acceleration: (a) time domain, (b) time-frequency map under road excitation, and (c) time-frequency map under coupling excitation.
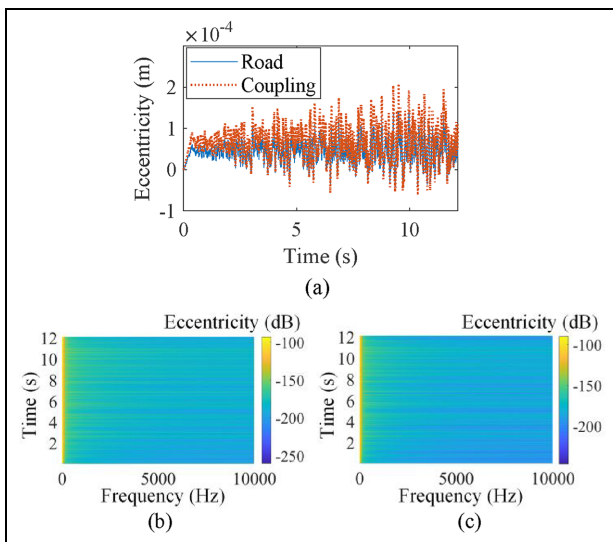

Figure 13. Motor eccentricity: (a) time domain, (b) time-frequency map under road excitation, and (c) time-frequency map under coupling excitation.

Figure 15. Vehicle body pitch angle acceleration: (a) time domain, (b) time-frequency map under road excitation, and (c) time-frequency map under coupling excitation.

$f_s \pm 3f_c, f_s \pm 9f_c$, the rotor vertical vibration mainly occurs at $f_s \pm 3f_c$ and $3f_s \pm 3f_c$, which are consistent with the frequency components of UMFs shown in Figure 4. The influence of UMFs on the vertical vibration of vehicle body and stator is obvious. Due to the damping effect of suspension, there is no obvious difference in the time-frequency maps of vehicle body vertical acceleration under road excitation and coupling excitation in the high frequency range.

The vehicle body longitudinal acceleration and vehicle body pitch angle acceleration under road excitation and coupling excitation are shown in Figures 14 and 15. From the time domain, the vehicle body longitudinal acceleration and vehicle body pitch angle
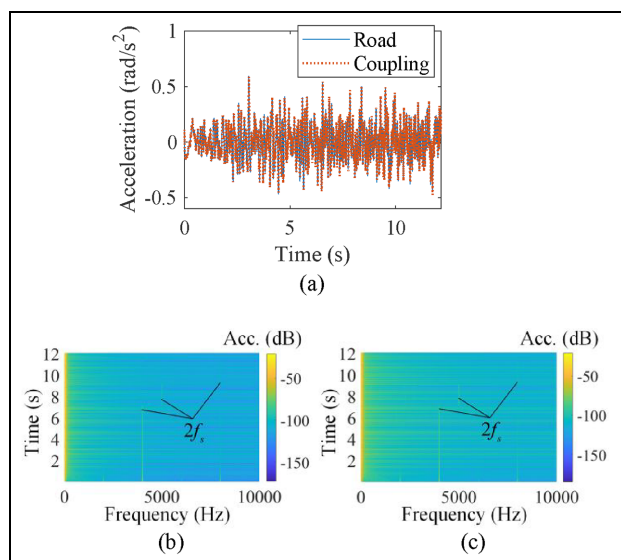
acceleration fluctuate more strongly with the increase of vehicle speed (motor speed). The UMFs have little effect on the vehicle body longitudinal acceleration and vehicle body pitch angle acceleration. In time-frequency maps, the main harmonics of vehicle body longitudinal acceleration are $f_s \pm 3f_c$ and $2f_s$, the main harmonic of vehicle body pitch angle acceleration is $2f_s$. There is no obvious difference in the frequency characteristics of vehicle body longitudinal acceleration under road excitation and coupling excitation, so is the vehicle body pitch angle acceleration.

Figure 16 shows the time-frequency map of hub motor electromagnetic torque under acceleration condition, it exhibits order features obviously. The main
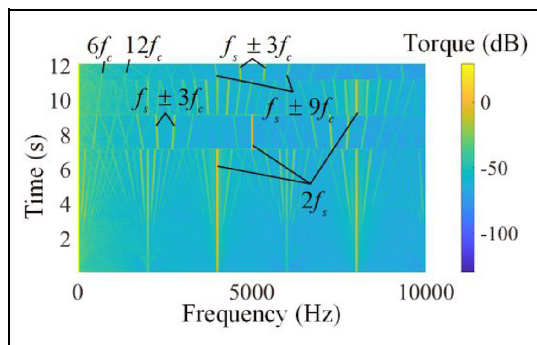
Figure 16. Time-frequency map of hub motor electromagnetic torque.

harmonics are $6f_c$, $12f_c$, $f_s \pm 3f_c$, $f_s \pm 9f_c$, and $2f_s$, which are consistent with the $2f_s$ in the time-frequency maps of vehicle body pitch angle acceleration and tire longitudinal force, and with the $f_s \pm 3f_c$ and $2f_s$ in the time-frequency maps of vehicle body longitudinal acceleration. Therefore, it can be concluded that the harmonics in the time-frequency maps of vehicle body longitudinal acceleration and vehicle body pitch angle acceleration are caused by the hub motor electromagnetic torque. The hub motor electromagnetic torque exists under both road excitation and coupling excitation, so there is no obvious difference in the time-frequency maps under road excitation and coupling excitation.

Conclusion

In this paper, a longitudinal-vertical coupling dynamics model has been established, and the longitudinal-vertical coupling vibration characteristics of the four hub motors driven electric vehicle under road excitation and coupling excitation was analyzed. The accuracy of the longitudinal-vertical coupling dynamics model was verified by acceleration test of the four hub motors driven electric vehicle. Some conclusions can be obtained from this paper.

(1) The longitudinal and vertical movement of the four hub motors driven electric vehicle is coupled by hub motor. The tire longitudinal force of the hub motor is the driving force of the electric vehicle. The change of tire longitudinal force requires the change of motor electromagnetic torque, which affects the motor currents, resulting in the change of hub motor UMFs. The UMFs act on the hub motor stator and rotor parts, which will affect the vertical vibration of the electric vehicle and cause the change of wheel vertical load. The change of wheel vertical load will affect tire longitudinal force which can be seen from the tire model, that is, there is longitudinal-vertical coupling in the four hub motors driven electric vehicle.

(2) The influence of UMFs on the dynamic behavior of the electric vehicle is mainly reflected in the vertical vibration of vehicle body and motor stator. Under acceleration condition, the UMFs of the hub motor leads to the vertical vibration of vehicle body and motor stator, the vibration frequency show obvious low order harmonic hf_c and the inverter switching frequency sideband harmonic $k_1 f_s \pm k_2 f_c$. Due to the damping effect of suspension, there is no obvious difference of vehicle body vertical acceleration under road excitation and coupling excitation in the high frequency range.

(3) The electromagnetic torque of the hub motor has influence on the vehicle body longitudinal vibration and the vehicle body pitch angle acceleration. Electromagnetic torque of the hub motor leads to the longitudinal vibration of the vehicle body, the main harmonics are $f_s \pm 3f_c$ and $2f_s$. The main harmonic of the vehicle body pitch angle acceleration is $2f_s$.

The research in this article can better predict or explain the order vibration of the hub motors driven electric vehicle, and provide a theoretical basis for mitigating the order vibration of the electric vehicle under unsteady condition.

Declaration of conflicting interests

The author(s) declared no potential conflicts of interest with respect to the research, authorship, and/or publication of this article.

Funding

ORCID iDs

Conggan Ma https://orcid.org/0000-0002-0292-7702
Yue Guo https://orcid.org/0000-0003-3073-8092

References

1. Wu Z, Zuo S, Huang Z, et al. Modelling, calculation and analysis of electromagnetic force and vibroacoustic behavior of integer-slot permanent magnet synchronous motor considering current harmonics. *J Vib Eng Technol* 2022; 10(3): 1135–1152.
2. Liu M, Zhang Y, Huang J, et al. Optimization control for dynamic vibration absorbers and active suspensions of in-wheel-motor-driven electric vehicles. *Proc IMechE, Part D: J Automobile Engineering* 2020; 234(9): 2377–2392.
3. Tian M and Gao B. Dynamics analysis of a novel in-wheel powertrain system combined with dynamic vibration absorber. *Mech Mach Theory* 2021; 156: 1–21.

4. Luo Y and Tan D. Study on the dynamics of the in-wheel motor system. *IEEE Trans Vehicular Technol* 2012; 61(8): 3510–3518.

5. Tan D, Song F and Wang Q. Design and optimization of the in-wheel motor driving electric vehicle based on the vibration energy transmission. *J Vib Control* 2017; 24(21): 5129–5140.

6. Wang Q, Li R, Zhu Y, et al. Integration design and parameter optimization for a novel in-wheel motor with dynamic vibration absorbers. *J Braz Soc Mech Sci Eng* 2020; 42: 459.

7. Meng L, Zou Y, Qin Y, et al. A new electric wheel and optimization on its suspension parameters. *Proc IMechE, Part D: J Automobile Engineering* 2020; 234(12): 2759–2770.

8. Drexler D and Hou ZC. Simulation analysis on vertical vehicle dynamics of three in-wheel motor drive configurations. *Proc IMechE, Part D: J Automobile Engineering* 2023; 1–15.[AQ: 2]

9. Zuo S, Li D, Mao Y, et al. Longitudinal vibration analysis and suppression of electric wheel system driven by in-wheel motor considering unbalanced magnetic pull. *Proc IMechE, Part D: J Automobile Engineering* 2019; 233(11): 2729–2745.

10. Wu H, Zheng L and Li Y. Coupling effects in hub motor and optimization for active suspension system to improve the vehicle and the motor performance. *J Sound Vib* 2020; 482.[AQ: 3]

11. Zhao P and Fan Z. Optimisation of electric vehicle with the in-wheel motor as a dynamic vibration absorber considering ride comfort and motor vibration based on particle swarm algorithm. *Proc IMechE, Part K: J Multi-body Dynamics* 2023; 237(1): 49–59.

12. Hu Y, Li Y, Li Z, et al. Analysis and suppression of in-wheel motor electromagnetic excitation of iwm-ev. *Proc IMechE, Part D: J Automobile Engineering* 2021; 235(6): 1552–1572.

13. Yamada S, Beauduin T, Fujimoto H, et al. Active model-based suppression of secondary ride for electric vehicles with in-wheel motors. *IEEE/ASME Trans Mechatron* 2022; 27(6): 5637–5646.

14. Kopylov S, Phanomchoeng G, Ambrož M, et al. Improvements to a vehicle's ride comfort by controlling the vertical component of the driving force based on in-wheel motors. *J Vib Control* 2023; 29: 4001–4014.

15. Vidal V, Stano P, Tavolo G, et al. On Pre-Emptive In-Wheel motor control for reducing the longitudinal acceleration oscillations caused by road irregularities. *IEEE Trans Vehicular Technol* 2022; 71(9): 9322–9337.

16. Jin X, Wang J, He X, et al. Improving vibration performance of electric vehicles based on in-wheel motor-active suspension system via robust finite frequency control. *IEEE Trans Intell Transp Syst* 2023; 24(2): 1–13.

17. Tan D and Lu C. The influence of the magnetic force generated by the in-wheel motor on the vertical and lateral coupling dynamics of electric vehicles. *IEEE Trans Vehicular Technol* 2016; 65(6): 4655–4668.

18. Wang YY, Li YN, Sun W, et al. Effect of the unbalanced vertical force of a switched reluctance motor on the stability and the comfort of an in-wheel motor electric vehicle. *Proc IMechE, Part D: J Automobile Engineering* 2015; 229(12): 1569–1584.

19. Yu Y, Zhao L and Zhou C. Influence of rotor-bearing coupling vibration on dynamic behavior of electric vehicle driven by inwheel motor. *IEEE Access* 2019; 7: 63540–63549.

20. Shao X, Naghdy F, Du H, et al. Coupling effect between road excitation and an in-wheel switched reluctance motor on vehicle ride comfort and active suspension control. *J Sound Vib* 2019; 443: 683–702.

21. Wang Y, Li P and Ren G. Electric vehicles with in-wheel switched reluctance motors: coupling effects between road excitation and the unbalanced radial force. *J Sound Vib* 2016; 372: 69–81.

22. Li Z, Zheng L, Gao W, et al. Electromechanical coupling mechanism and control strategy for in-wheel-motor-driven electric vehicles. *IEEE Trans Ind Electron* 2019; 66(6): 4524–4533.

23. Ma C, Cui H, Zheng P, et al. Influence of static eccentricity on unbalanced magnetic force of external rotor permanent magnet brushless direct current motor used as in-wheel motor. *IET Electric Power Appl* 2019; 13(4): 538–550.

24. Deng W and Zuo S. Comparative study of sideband electromagnetic force in internal and external rotor PMSMs with SVPWM technique. *IEEE Trans Ind Electron* 2019; 66(2): 956–966.

25. Sun W, Li Y, Huang J, et al. Vibration effect and control of inwheel switched reluctance motor for electric vehicle. *J Sound Vib* 2015; 338: 105–120.

26. Mao Y, Zuo S and Wu X. Longitudinal vibration analysis of electric wheel system in starting condition. *SAE Int J Veh Dyn Stab NVH* 2017; 1(2): 156–164.

27. Mao Y, Zuo S, Wu X, et al. High frequency vibration characteristics of electric wheel system under in-wheel motor torque ripple. *J Sound Vib* 2017; 400: 442–456.

28. Mao Y, Zuo S and Cao J. Effects of rotor position error on longitudinal vibration of electric wheel system in in-wheel PMSM driven vehicle. *IEEE/ASME Trans Mechatron* 2018; 23(3): 1314–1325.

29. Zuo S, Hu X, Li D, et al. Analysis and suppression of longitudinal vibration of electric wheel system considering rotor position error. *IEEE Trans Transp Electrification* 2021; 7(2): 671–682.

30. Pacejka H (ed.). *Tire and vehicle dynamics*. 3rd ed. Oxford: Butterworth-Heinemann, 2012.